A Transient Simulation and Dynamic Spray Cooling Control Model for Continuous Steel Casting

RICHARD A. HARDIN, KAI LIU, ATUL KAPOOR, and CHRISTOPH BECKERMANN

A two-dimensional heat-transfer model for transient simulation and control of a continuous steel slab caster is presented. Slab temperature and solidification are computed by the model as a function of time-varying casting speed, secondary spray cooling water flow rates and temperature, slab thickness, steel chemistry, and pouring and ambient temperatures. Typically, the solidification path, temperature-solid fraction relationship, is prescribed. However, if these data are not available, a microsegregation solidification model that approximates the effects of steel chemistry and cooling rate is incorporated in the caster model. Measured slab surface temperatures recorded from an operating caster are compared with predictions from the transient model. These demonstrate that the model typically can predict the temperature response at the slab surface within 30 °C. Results of several simulations are given to demonstrate the effects of changing casting conditions on the slab thermal profile, end of liquid pool, and solidification end point. A control methodology and algorithm suitable for online control of a continuous casting machine is described, and the ability to control the surface temperature profile by dynamically adjusting secondary spray cooling flow rates is demonstrated by simulation. Results from a preliminary version of the model that is capable of running in real time are presented and are compared with the slower, but more realistic, version of the model.

I. INTRODUCTION

IN order to remain competitive in the worldwide market for continuously cast steel, steel producers are finding it increasingly important to implement process control improvements. Through superior production process monitoring and control, producers are improving steel quality and are meeting customers' requirements for steel size, grade, quantity, and properties at the lowest cost. Computer models used for real-time/online prediction and control of continuous steel casters are fundamental tools in this effort. Accurate online prediction and control allows for flexibility in caster operation. It gives operators the capability to vary casting speeds while keeping process parameters such as slab surface temperatures and solidification end point within desired ranges. Such control capability results in more uniform cast material throughout an entire casting sequence. Leaving aside the benefits of online/real-time control models, offline transient modeling gives insight into the time-varying behavior of process variables and parameters, and a more thorough understanding of the casting process.

The simplest method of caster spray cooling control is to deliver a prescribed amount of water flow that is proportional to the casting speed. Different proportions of flow to casting speed are delivered to the casting machine's spray cooling water flow loops. These flow loops supply water to banks of spray nozzles that are arranged into spray cooling zones. Usually, these zones are assigned to a machine segment, or combination of segments, and are often divided into spray banks on the top and bottom slab surfaces. The use of water flows that are proportional to casting speed can be improved somewhat by prescribing the spray zone flows as nonlinear functions of casting speed. These relationships between water flow and casting speed are determined by experience, measurement, or steady state modeling so that the slab temperature at steady state is maintained within a desired range for all casting speeds.

Regardless of the relationship between water flow and casting speed, the practice of controlling the water flow based directly on the casting speed results in transient variations in the slab temperature even if the slab returns to a desirable thermal condition at steady state. In order to prevent such temperature excursions, even during caster startup and shutdown, the spray cooling water must be controlled dynamically. In dynamic spray cooling control, the spray water flow is continuously controlled during transient changes in caster operation to maintain the desired thermal conditions throughout the steel slab at all times. Due to the unreliability of temperature sensors, the lack of good sensors for important process parameters such as liquid pool depth (the point in the caster where the final phase change from pure liquid to liquid-solid mush occurs), and solidification end point (the point in the caster where the final phase change from liquid-solid mush to pure solid occurs), computer-based control models represent the best, if not only, method for reliable dynamic control.

When the objective of transient simulation is real-time control, typically, the physical model must be simplified. Thermal tracking of the slab cooling history is probably the most time-tested method of dynamic control of continuous casters, but it involves simplification. This method of control is described by Irving.[1] The heat-transfer coefficient is correlated to the spray cooling water flux. Using this correlation, the thermal histories of segments of the slab are "tracked" over time, and the spray water is controlled to achieve a prescribed heat-transfer coefficient-time relationship. This heat-transfer coefficient-time relationship is established

RICHARD A. HARDIN, Assistant Research Engineer, KAI LIU, Research Assistant, and CHRISTOPH BECKERMANN, Professor, are with the Department of Mechanical and Industrial Engineering, The University of Iowa, Iowa City, IA 52242–1527. Contact e-mail: becker@engineering.uiowa.edu ATUL KAPOOR, formerly Research Engineer, IPSCO Saskatchewan Inc., Regina, SK, Canada S4P 3C7, is Senior Consultant, Cap Gemini Ernst and Young Canada Inc., Toronto, ON, Canada M5K 1J5.

Manuscript submitted September 17, 2002.

based on maintaining the temperature profile of the slab. Okuno *et al.*[2] present a real-time computer model–based secondary spray cooling control system based on tracking the temperatures at planes of the steel slab in real time and predicting the water flow rate required to maintain set-point surface temperatures at four "control points" along the caster length. The control points are positioned immediately after the spray banks to be controlled. Model calculations are performed every 20 seconds. Feedback sensors are used to calibrate the system and to assist in recalculating spray water flow rates when the surface temperatures at the four control points are in agreement with the control points' target temperatures. Spitzer *et al.*[3] present a model that has been used on several casters to control dynamic spray cooling based on tracking slab slices. Here, online temperature measurements are used along with a solution of the inverse heat conduction problem to adjust the heat-transfer coefficients to better control the slab surface temperatures at five set points. Agreement between model and measured surface temperatures was within 30 °C when the online measurements were used to adjust the model's heat-transfer coefficients, and it was within 50 °C when no corrections were used.

Another approach to dynamic spray cooling modeling and control was developed by Barozzi *et al.*[4] in which the allowable surface temperature ranges at several setpoints, shell thickness, and mean exit temperature from the machine are all weighted to control both water flow rates and casting speed. This model uses a combined feedback and feed-forward technique to control the temperatures at end-zone locations. Here, the feedback-controlled variable is not a measured temperature, but a temperature computed by a dynamic real-time model. A feed-forward loop is applied to calculate the heat flow required to reach the desired set point from the computed surface temperature, and the water flow rates are adjusted based on this estimation. Separate computational domains are used for the solid shell region, and the solidifying mushy region. The two regions are coupled by applying continuity of heat flow across their boundaries. The equation describing the solidifying region is reduced to an ordinary differential equation by assuming a parabolic temperature profile across it, and heat conduction is solved in the solid shell. While the approximations in this model were necessary given the computational capabilities at the time of its development, the solidification and release of latent heat cannot be modeled as accurately here as it can in a physics-based heat-transfer/solidification model. The power of computation now allows us to use models for caster control that are based on physics and metallurgical principles without such approximations. The model used in the present work can accurately predict the solidification process for the wide range of cooling rates inherent in the continuous casting process, and it can be verified by comparison with experimental data outside the control model.

A real-time transient heat-transfer model for continuous casting is presented by Louhenkilpi *et al.*,[5] with example results given for a machine casting stainless steel. This model uses a prescribed nonlinear solid fraction *vs* temperature relationship calculated by a solidification model based on steel grade. Temperature-solid fraction relationship and steel properties are computed using the model developed by Miettinen[6] and Miettinen and Louhenkilpi.[7] Spray cooling correlations depend upon several variables (spray water flux, slab surface temperature, spray cooling zone number, and steel grade), and were determined from a curve fitting procedure based on measured temperatures. Louhenkilpi[8] has also developed an online model for solidification end point prediction and a dynamic spray cooling control system (CASIM). Tracking of the residence time of slices of the slab in the caster and look-up tables for solidification end point *vs* cooling history (computed by a steady-state model) are used to control the position of the solidification end point in the CASIM model. Also, a control model called DYNCOOL has been developed by Louhenkilpi based on the real-time model.[5] Other examples of online secondary spray cooling control systems reported in the literature are those developed by Voest-Alpine Industrieanlagenbau (VAI)[9] and Sumitomo Metals.[10]

Computational capabilities have now progressed to the point where models used in casting process control will include fewer physical simplifications. In the present work, the dynamic spray cooling simulator (DYSCOS) model was developed for continuous casters at IPSCO Inc. The DYSCOS simulates transient caster operation with and without dynamic spray cooling control. A distinguishing capability of this model is that DYSCOS is physics based and not limited or simplified for real-time control only. Therefore, it can be run as both an "offline" model, which is slower than real time but includes a high degree of detail, and as a real-time model, which can be used for "online" prediction and control. Because the same describing equations are used in the DYSCOS model for real-time and offline computations, the effects on model accuracy and execution speed can be explored given varying degrees of boundary condition and solidification modeling detail. For example, the effects of grid resolution and describing equations (such as including heat conduction in the casting direction or using a microsegregation based solidification model) on model predictions can be investigated. Presently, the real-time online control model operates using stored or "virtual" computer-generated casting conditions. It has yet to be trial tested on a caster.

II. MODEL DESCRIPTION AND FORMULATION

The DYSCOS model solves two-dimensional transient heat-transfer and solidification equations at the midwidth position of the slab, as shown in Figure 1(a). The boundary conditions applied to regions of the machine are shown in Figure 1(b). The offline DYSCOS model can be run in two modes: a "transient simulation" mode and a "control" mode. In the transient simulation mode, transient casting speed, water flow rates, pouring temperature, secondary spray water temperature, and ambient temperature are prescribed to the model *via* input file. Temperature and solidification process conditions in the slab are computed so that transient variations in important process conditions, such as changes in the liquid steel pool, solidification end point, and slab surface temperatures, are computed in response to the changing conditions. When used in the control mode, DYSCOS computes, applies, and records the spray cooling water flow rates required to maintain a prescribed surface temperature profile on the caster surface in response to changing conditions.

The most realistic predictions obtained from DYSCOS result from using a highly refined grid with detailed boundary conditions. For such cases using a 667 MHz Alpha 21164 processor (Microway, Inc., Plymouth, MA), the model operates at execution speeds 20 times slower than real time.

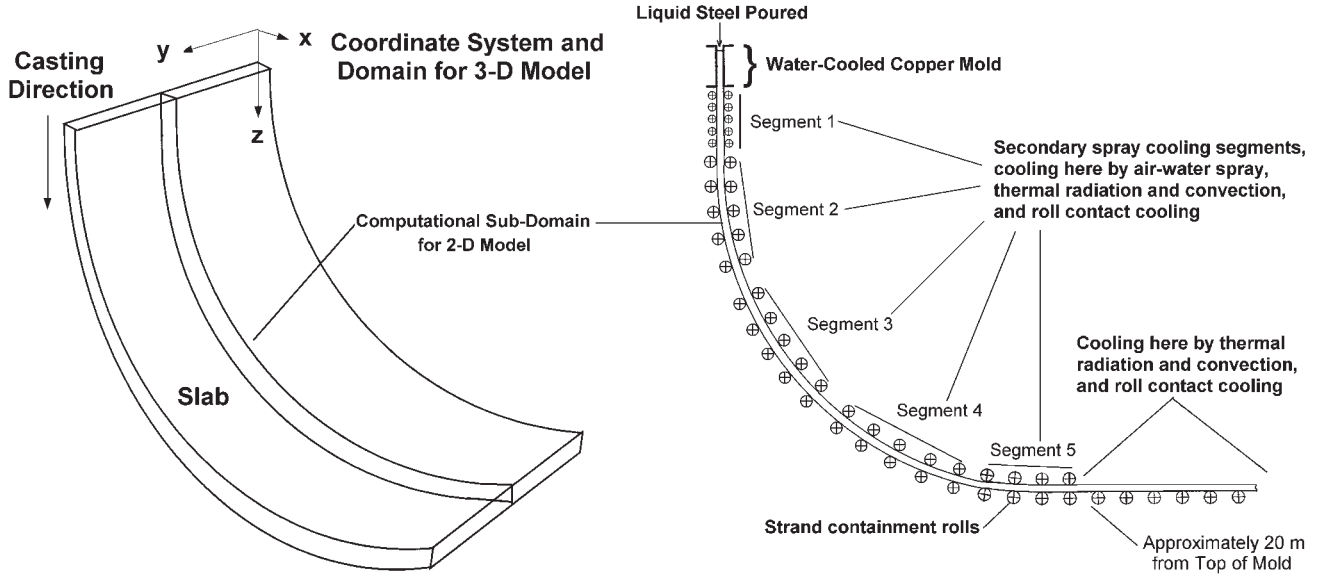

Fig. 1—(*a*) Schematic diagram of the coordinate system and calculation domain for the DYSCOS model and (*b*) diagram of boundary conditions used in the model.

In "Model Results" section, the reader will find more specific examples of computational requirements and execution speeds for various operating conditions. Results from this computationally intensive application of the model provide a realistic basis for testing control strategies and algorithms. Tradeoffs between computational speed and model accuracy for this and the coarser-grid real-time model can be evaluated. These comparisons can be used to demonstrate the degree of accuracy the real-time control model will have relative to the more accurate model. The more accurate model, termed the offline model, could be used to develop cooling control strategies. The offline model, once tuned, can be used instead of extensive trials on the actual machine. The real-time model, on the other hand, can be used as a virtual simulator or trainer for caster operations.

A. *Model Equations*

The energy equation describing two-dimensional transient heat transfer and solidification is solved by the DYSCOS program. The calculation domain, shown in Figure 1, is a thickness section taken through the midwidth of the slab. This domain extends from the meniscus to a predetermined distance down to the caster. In order to reduce computation time, symmetry at the centerline of the slab thickness can be assumed. In such a case, only the top surface boundary conditions of the slab are considered. Melt convection is not directly modeled; the additional energy transport due to convection is approximated through a thermal conductivity enhancement factor that is a function of the solid fraction. In continuous casting of steel under typical processing conditions, the axial-direction conduction term is generally much smaller than the shell thickness conduction and casting speed advection terms. Nevertheless, axial conduction is computed by the DYSCOS model. This makes the model applicable to continuous casting of higher thermal conductivity materials and usable at very low casting speeds. Comparative studies with and without axial conduction using the DYSCOS model have shown that the results are not appreciably different for normal steel casting conditions and properties.

The energy equation describing the preceding situation is

$$\rho c_p \left(\frac{\partial T}{\partial t} + V_{\text{cast}} \frac{\partial T}{\partial z} \right) = \frac{\partial}{\partial x} \left(k_{\text{eff}} \frac{\partial T}{\partial x} \right) + \frac{\partial}{\partial z} \left(k_{\text{eff}} \frac{\partial T}{\partial z} \right) + S \qquad [1]$$

where

$$\rho c_p = \varepsilon \, \rho_s \, c_{ps} + (1 - \varepsilon) \rho_1 c_{p1}$$

$$k_{\text{eff}} = [k_s \varepsilon + (1 - \varepsilon) \, k_1][1 + \beta (1 - \varepsilon)^2]$$

$$S = \Delta h \left(\frac{\partial (\varepsilon \rho_s)}{\partial t} + V_{\text{cast}} \frac{\partial (\varepsilon \rho_s)}{\partial z} \right)$$

and where ρ, c_p, T, t, V_{cast}, z, x, k, ε, β, and Δh are the density, specific heat, temperature, time, casting speed, casting direction, thickness direction, thermal conductivity, solid volume fraction, thermal conductivity enhancement factor, and latent heat, respectively. The subscripts *s*, *1*, ref, and eff denote solid, liquid, reference, and effective, respectively. The first term on the left-hand side of Eq. [1] accounts for transient effects, and the energy transported down the slab with the casting speed is taken into account by the second term. The first term on the right side is the *x*-direction (thickness) conduction term, and the second term is the *z*-direction (axial) heat conduction term. The last term on the right side accounts for the latent heat released during the solidification process, as described subsequently. Temperature-dependent steel property data from Pehlke *et al.*[11] are used through curve-fit functions for three categories of low alloy steels having medium (0.15 < wt. pct C < 0.45), high (wt. pct C > 0.5), and low (wt. pct C < 0.08) carbon contents.

Alternatively, temperature-dependent property data may be provided using a file.

A microsegregation model for multicomponent steel solidification is incorporated into DYSCOS. This microsegregation solidification model is described in more detail elsewhere.[12] This capability enables the temperature-solid fraction relationship to be computed for a given steel chemistry in cases where the solidification path data are not available, or when one is investigating the effects of cooling rate on solidification and microsegregation. The evolution of the temperature and solid fraction is computed in each computational cell, by coupling the energy equation to chemical species conservation and back-diffusion microsegregation model equations. Data for 15 alloying elements are included in the DYSCOS model database, and the dependence of the liquidus temperature on liquid species concentration is obtained by using the functions given by Howe.[13] The approach taken by Schneider and Beckermann[14] is used to model the back-diffusion. This is based on the assumption of a one-dimensional platelike dendrite arm geometry and a parabolic concentration distribution in the dendrite arm.[15] It has been shown[16] that this microscopic solute diffusion model has an analytical solution for the liquid concentration when a single solute is present and a parabolic solidification rate is assumed. This solution depends upon ε (the solid fraction), κ (the partition coefficient), and a diffusion Fourier number $\mathrm{Fo} = 4D_s t_s/\lambda$, where t_s is the local solidification time, D_s is the diffusivity of the species in the solid, and λ is the secondary dendrite arm spacing. For large values of Fo (high mass diffusivity, small dendrite arm spacing, or very long solidification time), this solution reduces to the lever rule, and for small vales of Fo, it reduces to the Scheil model.[16]

It has been shown in Reference 12 that this solidification model adequately predicts the liquidus and solidus temperatures when compared to the measurements published by Jernkontoret.[17] This model also produces temperature-solid fraction curves that compare well with the Interdendritic Solidification model (IDS) developed for Steel by Miettinen[6] for low alloy steels of similar composition to that cast on the machines for which the model was developed. When using this solidification model, temperature and solid fraction in each computational cell are determined through iterations between the energy Eq. [1], the overall species conservation equation for each species, the solid-species diffusion equation, and the liquidus temperature equation. These are coupled using Newton–Raphson iterations to determine the solid fraction and temperature during solidification of a computational volume. Generally, prescribing a temperature-solid fraction curve remains the recommended and fastest computational approach. The discretized equations are solved using the finite volume method and a tri-diagonal matrix algorithm solver with alternating direction implicit sweeping.

B. *Initial and Boundary Conditions, and Properties*

For initial conditions, the DYSCOS model assumes that the caster is in operation under steady-state conditions, and that steel slab is present throughout the machine. Output from a steady-state model, Caster-GUI, is used to prescribe the initial temperature and solid fraction distributions. A version of the Caster-GUI model is discussed elsewhere.[18] It was not envisioned that the DYSCOS model would predict the caster startup or shutdown processes; however, it will be shown to have good accuracy in those processes also.

Calibrating and determining the proper boundary conditions for a continuous casting machine can be difficult due to the multiple modes of heat transfer involved. Also, there are extraneous variables on an industrial machine that are difficult to take into account. In the mold region, an average heat flux as a function of dwell time is used in DYSCOS based on in-plant measurements. Thermal radiation is computed over the entire casting surface after the exit of the mold, except at roll contact points. The surface emissivity for steel is taken to be a function of temperature determined from the data compiled by Touloukian *et al.*[18] For the steels similar to those that the model is applied to,[18] the emissivity as a function of surface temperature is given by

$$\varepsilon = \frac{0.85}{[1 + \exp\,(42.68 - 0.02682\,T_{\mathrm{surface}})^{0.0115}]} \qquad [2]$$

where T_{surface} is in Kelvin. A Newtonian heat-transfer coefficient was then used to compute radiation heat transfer between the slab surface and the ambient caster temperature:

$$h_{\mathrm{rad}} = \varepsilon\sigma\left(T_{\mathrm{surface}}^2 + T_{\mathrm{ambient}}^2\right)(T_{\mathrm{surface}} + T_{\mathrm{ambient}}) \qquad [3]$$

where T_{surface} and T_{ambient} are in Kelvin. In regions of secondary cooling spray, heat-transfer coefficients are calculated using the of Nozaki *et al.*[19]

$$h_{\mathrm{spray}} = \frac{1570\dot{w}^{0.55}(1 - 0.0075\,T_{\mathrm{spray}})}{\alpha} \qquad [4]$$

where $\dot{w}$ is the spray cooling flux (L/m^2 s), T_{spray} is the temperature of the spray cooling water (°C), α is a machine-dependent calibration factor, and h_{spray} is the spray cooling heat-transfer coefficient (W/m^2 K). For the downward facing surface, the coefficient is modified to include the effect of orientation by multiplying Eq. [4] by $(1 - 0.15\cos\theta)$, where θ is the slab surface angle from horizontal. This modification for the downward facing surface is based on the measurements by Bolle and Moureau,[20] who measured a 15 pct decrease in spray cooling for a downward facing slab surface relative to the upward facing surface.

Temperature measurements were taken during normal caster operation at points at the center slab span on the upper surface to determine the α calibration constants. The α values were determined by automated iterative calculations, adjusting h_{spray} over the corresponding length of the machine until the steady-state caster model results agreed with the surface temperature measurements. The iterated h_{spray} values are determined using Newton's method and a solution for h_{spray} is found usually within seven iterations. The α constant will vary on the machine owing to the distribution of spray and layout of the spray nozzles, and other extraneous variables. For the caster on which the measurements presented in this article were made, three constants were determined over three regions of the machine, using pyrometers positioned at three locations. These regions were mold exit to 7.44 m from meniscus, 7.44 to 9.16 m from meniscus, and 9.16 to 18.45 m from meniscus. Using several weeks of steady-state data collected on-line by IPSCO Inc., the α calibration constants for this machine were found to be 3.5, 3.17, and 5.42 at the three respective pyrometer locations, as shown in

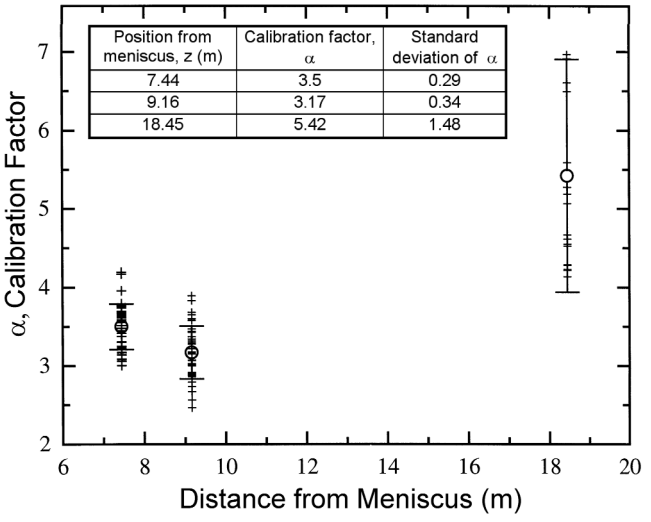

Fig. 2—Spray cooling calibration α factors determined from matching simulated and measured surface temperatures; also shown are mean and standard deviations.

Figure 2. The α calibration constant data given in Figure 2 results from a range of steel chemistries and casting conditions; hence, there is some scatter. If only one α constant were used over the entire machine length, the average α would be about 4.4. These findings appear reasonable given that Nozaki *et al.*[19] used a value of $\alpha = 4$ and that Laitinen and Neittaanmäki[21] used α values of 5 and 6 in the same correlation. The model has also been applied to a second IPSCO Inc. caster on which only limited temperature data are available. On this machine, a single calibration constant of $\alpha = 4$ was used for the entire length of the machine used, in keeping with the original correlation developed by Nozaki *et al.*[19] Subsequently, on this machine, surface temperature predictions were found to be in good agreement with limited handheld pyrometer measurements taken after the secondary spray zones.

At the roll contact points, the heat-transfer coefficients are determined from measurements in the literature.[22,23] An effective roll contact length of 10 pct of the roll diameter has been found to give good agreement with surface temperature oscillations observed[22,23] due to roll contact cooling. Where there is no spray or roll contact, a natural convection heat-transfer coefficient correlation is used:

$$h_{\text{nat}} = 0.84\,(T_{\text{surface}} - T_{\text{ambient}})^{1/3} \qquad [5]$$

where h_{nat} is the natural convection heat-transfer coefficient ($\text{W/m}^2\,\text{K}$), and T_{surface} and T_{ambient} are slab surface and ambient temperatures (K), respectively. This correlation was used previously to compute h_{nat} in continuous caster modeling.[24] Equation [13] results from assuming turbulent natural convection at an air film temperature of about 1050 K.[25] For the downward facing surface inclined at an angle from the gravitational direction, the effect of orientation is accounted for by multiplying the temperature difference by the cosine of the angle from the vertical. Even if natural convection heat transfer were considered in more detail, by using temperature-dependent properties, for instance, its effect on total cooling would be negligible. For the coarse-grid real-time model, the overall heat-transfer coefficient is determined from an area-weighted average of all heat-transfer

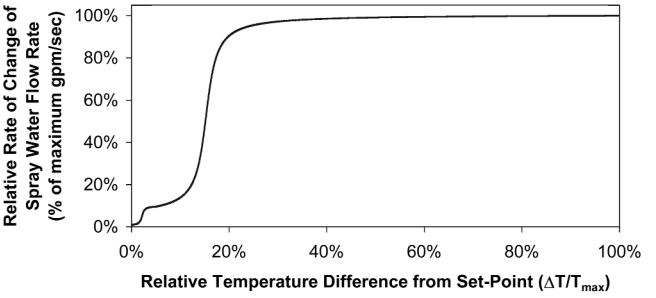

Fig. 3—Control function: rate of water flow rate change (relative to a maximum value) *vs* absolute relative difference from set-point temperature.

modes for each segment of the machine. More discussion of the properties and the boundary conditions used is given elsewhere.[12]

C. *Control Methodology and Algorithm*

Using the DYSCOS model, numerous control methodologies were tested for their capability to maintain a prescribed slab surface temperature profile along the caster. Such a control system should maintain temperatures at set points that are positioned near the end of the spray cooling zones on the machine, with one set point used to control each secondary spray water loop. To accomplish this, various control-module subprograms were implemented in the transient DYSCOS model. Then, the controlled water flow rates from the subprograms are used instead of the prescribed flow rates in the simulations. Traditional feedback and proportional control techniques failed to control the temperatures as well as desired. Based on computational experiments and parametric studies, a control function was established to control the rate of change in water flow rate as a function of the difference between the slab surface temperature from the desired set-point temperature. This difference between the predicted surface temperature and the set-point value is denoted by ΔT. The shape of the function found to give the best performance in terms of stability and response time is shown in Figure 3.

The flow rate of the zone corresponding to a given set point is varied as a function of the set-point temperature's difference from the desired value. The resulting change in flow rate applied by the control system is also dependent on the set-point monitoring rate in determining the rate of flow rate change. The same function is used to increase the water flow rate when the temperature is above the set point, or alternatively decrease the water flow rate when the temperature is below the set point. To prevent overshooting, the main cause of fluctuation in the temperature during control, some control logic is used to determine if a change in the water flow rate is to be made. The judgment used is this: when the temperature change is such that it approaches the set-point temperature, no change will be made in the water flow rate. A change in the water flow rate will be made only if the simulation temperature is moving away from the set-point temperature. In applying this control method to an actual caster, sensors are not required for feedback, but should be strategically used for safety and online calibration of the computer model in implementation, as described in Reference 4.

III. MODEL RESULTS

A. *Typical Results*

Refinement and detail of the model's boundary conditions in the offline operation mode resolves the individual roll contact cooling. This requires that the grid spacing in the axial direction be on the order of 1 mm at the roll contacts. A grid of about 3000 axial cells by 100 thickness cells is typical for this application for a domain approximately 20-m long (axial) by 0.2-m thick. Run times for the high-detail model are found to depend on the changing casting conditions, with faster convergence being achieved for less variant conditions. Depending on the casting conditions, simulation times for a typical grid (100 by 2500 cells in the slab thickness and casting directions, respectively) can vary between factors of 4 to 20 times real time using a 667 MHz Alpha 21164 processor.

Shown in Figure 4 are example results for temperature and solid fraction distribution that are computed at each timestep. Here, results are given through a 152-mm-thick slab for the entire caster. In Figure 4(a), the temperature profiles on the surfaces and at the centerline of the slab are shown, and in Figure 4(b), the solid fraction distribution for a 152-mm-thick slab is shown. These results are a snapshot "taken" at one time during a typical simulation. Note in Figure 4(a) that the cooling at the rolls produces downward temperature spikes.

The real-time version of the model differs from the offline version; its grid is reduced by an order of magnitude in each direction and boundary condition detail is lost. When the model is run using such a coarse grid, the roll contact cooling and spray distributions are averaged over machine segments, which results in a smooth surface temperature profile and gradually changing thermal conditions. Details of the temperature fluctuations at the slab surface are lost. Typically, a prescribed temperature-solid fraction relationship is specified to increase execution speed and to achieve execution speeds that are actually faster than real time.

B. *Comparison of Predicted and Measured Temperatures*

Comparisons between measured and predicted transient surface temperature variations at two positions from the meniscus on the slab surface are given in Figures 5 and 6. Simulation conditions are taken from online data acquired by IPSCO Inc. during caster operation. The slab thickness being cast in both cases is 102 mm. In both figures, the measured surface temperature is initially recorded when the slab first

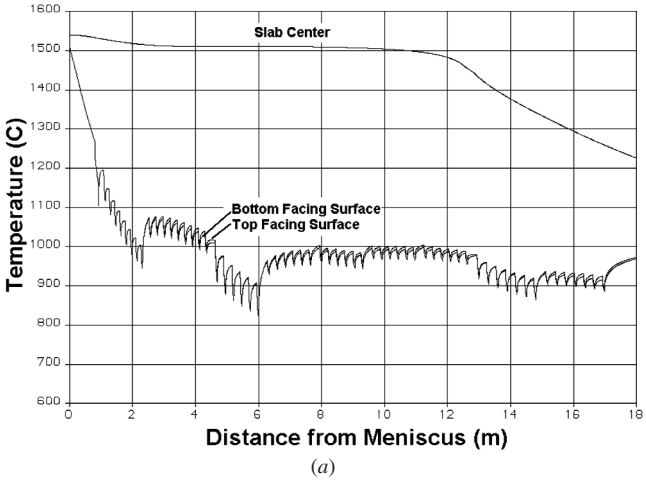

(*a*)

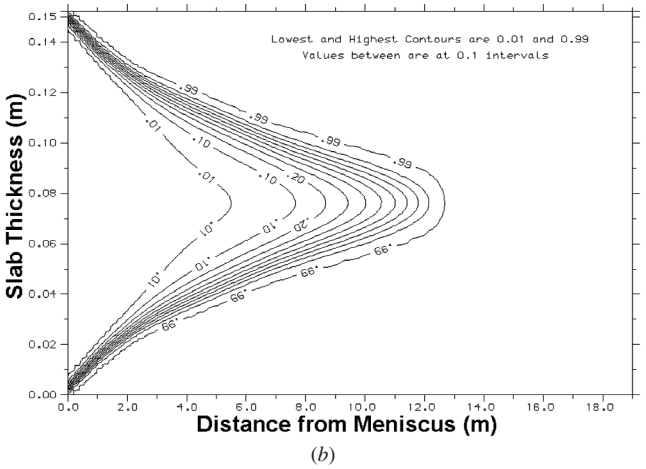

(*b*)

Fig. 4—(*a*) Temperature profile and (*b*) solid fraction distribution results from the high-detail DYSCOS model at an instant in time during a simulation.

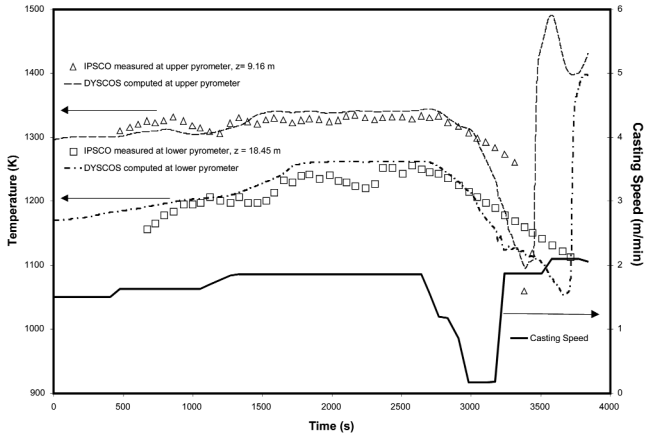

Fig. 5—Comparison between measured and predicted slab surface temperatures from the high-detail DYSCOS model with the casting speed conditions for a 102-mm-thick slab: case 1.

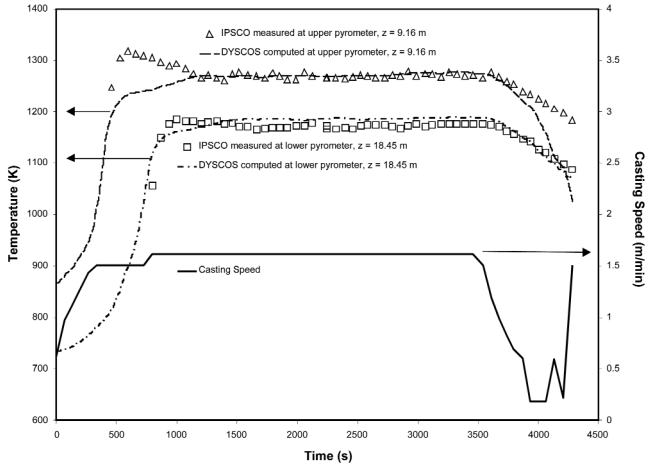

Fig. 6—Comparison between measured and predicted slab surface temperatures from the high-detail DYSCOS model with the casting speed conditions for a 102-mm-thick slab: case 2.

passes beneath the pyrometers as the caster begins operation at startup. In case 1, shown in Figure 5, the slab first passes the upper pyrometer (at 9.16 m from meniscus) at 459 seconds and the lower pyrometer (at 18.45 m from meniscus) at 795 seconds. There is good agreement with the measurements using the model calibration based on steady-state conditions. At the end of the casting sequence, the model tracks the initial drop in the temperature measurements due to the casting speed drop at about 2600 seconds. Here, note that the model appears to overpredict the initial part of the temperature drop that occurs at 3400 seconds. However, it captures the final temperature recorded at the end of the cast slab quite well. At the lower pyrometer, the model temperature is underpredicted by a maximum of 50 °C, but the prediction agrees very well with the data trend. In Figure 5, the model continues to predict the slab temperatures as if there were steel still in the machine. Hence, the predicted temperatures increase in response to the casting speed increase at about 3250 seconds. The measurements, on the other hand, are for a casting sequence, and they end when the last portion of slab passes the lowest pyrometer, at around 3700 seconds. Thus, one can disregard the predictions after the measurements end. Despite the fact that the model physics is not designed to predict temperatures in the "tail end" of the cast strand, it still compares rather well with the measurements. It predicts the interesting behavior of the measurements where the pyrometer temperature at 9.16 m drops dramatically below the measurements at 18.45 m. Note that the "time" at which the upper pyrometer measurement drops below the lower measurement is well predicted in the DYSCOS model. For case 2 (Figure 6), the startup process is predicted well by the model at the lower pyrometer position around 670 seconds as the first portion of slab passes the pyrometer. Realize the model starts with the assumption of a machine "full" of steel operating at steady state. The temperature drop that occurs following the casting speed decrease (at 3463 seconds) is overpredicted again by the model at 9.16 m, and this could be an indication that additional tuning of the spray correlation is needed. The difference could also be explained because these data are the 'tail end' of the slab for this cast sequence. However, there is a sharp temperature drop here, and, because there are no data beyond 4281 seconds, it is not known how well the DYSCOS model would have predicted the temperature trough for this case. If there were additional data, it might have been very similar to that seen in Figure 5.

C. *Control Algorithm and Results of Studies with and without Spray Cooling Control*

Parametric studies were performed to study the relative effects of casting variable changes on the surface temperatures and solidification conditions for the IPSCO casters. Increasing and decreasing casting speed, changing spray cooling water flow rates and temperatures, changing pouring temperature, and even changes in the caster environment temperature were investigated. Changes in the temperature profile and solidification end point, and the response time required to reach steady-state conditions, were among the most critical factors studied because they may affect slab quality. Not surprisingly, casting speed is the most important factor affecting thermal and solidification conditions. The response time of the caster to an increase in casting speed was observed to coincide with the time required for the new

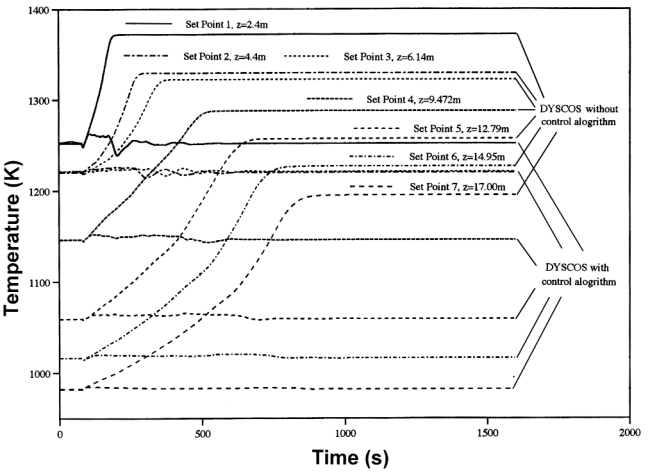

Fig. 7—Temperatures at set points for casting speed change from 0.7 to 1.2 m/min at 80 s with and without using spray cooling control for a 152-mm-thick slab.

conditions to propagate down the caster at the new casting speed. A longer response time than this propagation time is observed for a casting speed decrease. Results of several of these casting speed change studies will be discussed subsequently for cases with and without spray water control.

In Figure 7, results from an example case are given where the ability of the control module to maintain the initial temperatures at the control set points is demonstrated. Here, the casting speed is instantaneously stepped from 0.7 to 1.2 m/min at 80 seconds into the simulation. This is a rigorous test of the control method because casters not generally subject to such an abrupt speed increase due to the danger of breakouts. Near the top of the machine (at set point 1, for instance) the surface temperature is most difficult to control due to the higher temperatures and temperature fluctuations. Also given in this figure are the results of a parametric study on the effect of the same casting speed change with the water flow held constant. Note here that response times for the temperatures to reach steady state are observed to propagate at the new casting speed down the machine. The water flow rates generated by the control module to maintain the temperatures (for the 0.7 m/min casting speed) are given in Figure 8. Note the different rates of change of the flow rates in different zones of the machine. Also, these flow rates demonstrate that maintaining a constant temperature profile for this speed change is impractical for some locations, because the flow rates required for some zones are greater than the maximum allowable flow rates for the machine. In an online control module, flow limits and allowable surface temperature ranges should be added to the control logic, and the logic should include the ability to control the casting speed[4,24] in cases where water flow control alone will not suffice.

The solidification conditions inside the slab as represented by the depth of liquid pool (the final point above liquidus temperature) and solidification end point (the final point above solidus) change with casting speed despite control of the surface temperatures. Depending on the allowable range of these variables, limitations should be placed on the casting speed. In the present control scheme, the casting speed is limited by the maximum and minimum allowable solidification end point and liquid pool depth. As shown in

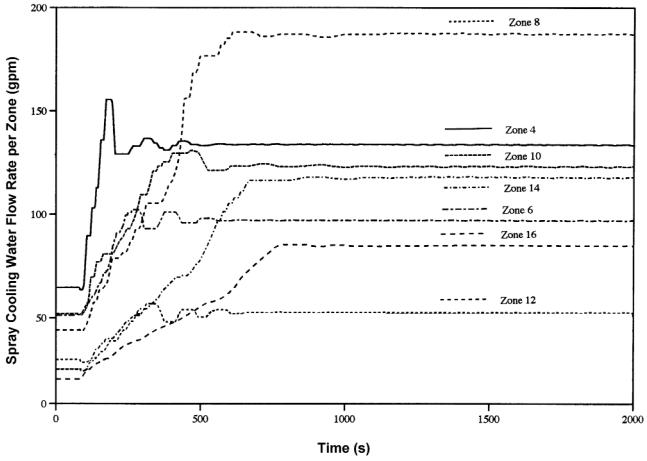

Fig. 8—Flow rates generated by DYSCOS control module for case with casting speed change from 0.7 to 1.2 m/min at 80 s for 152-mm-thick slab.

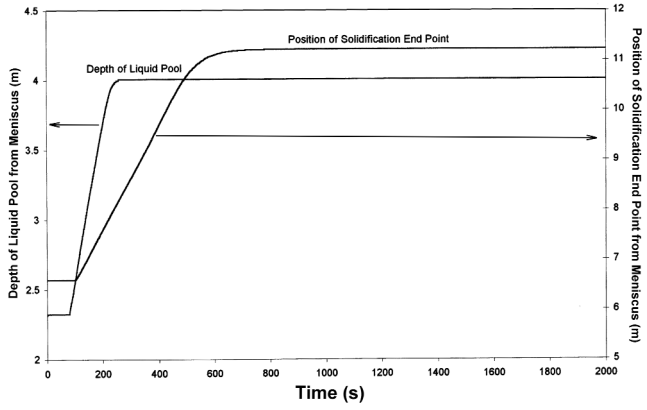

Fig. 9—Response of liquid pool depth and solidification end point to casting speed change from 0.7 to 1.2 m/min at 80 s for 152-mm-thick slab with control.

Figure 9 for the 0.7 to 1.2 m/min casting speed change with control, the time required for the liquid pool depth and solidification end point to respond corresponds to the time required for the new conditions to propagate at the new casting speed. The liquid pool settles to its new position approximately 200 seconds after the speed change, and the new position is at about $z = 4$ m. The time required for the new conditions to propagate 4 m into the machine is (4 m) ÷ (1.2 m/min) = 3.33 min = 200 s. For the solidification end point, the response time to the new solidification end point at 11.25 m is 563 seconds. This would correspond to 643 seconds in Figure 9, which appears to agree quite well with the computed result for solidification end-point response.

Slab surface temperatures at the control set points are given in Figure 10 for a decrease in casting speed occurring at 80 seconds into the simulation. Here, the casting speed is changed from 1.0 to 0.8 m/min. For the simulation without control, instead of keeping the flow rates constant in this case, the secondary cooling flows are adjusted according to a flow rate-casting speed lookup table (spray table). For the machines studied here, at present, the flows are controlled by the spray table method. The spray table gives one an instantaneous change in flow rate with casting speed, whereas the present control model continually adjusts it in each water flow loop. Temperature variations occur when the spray

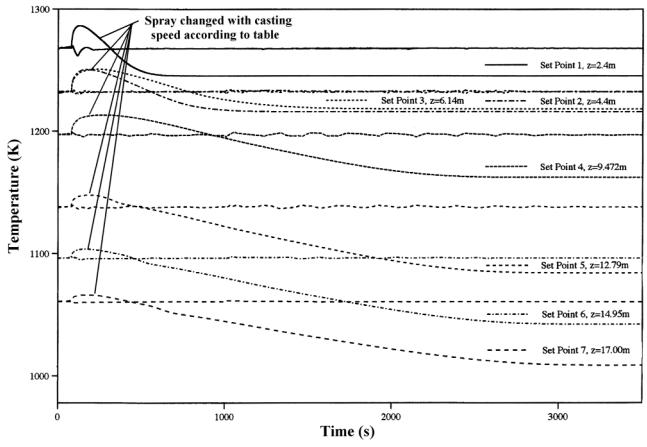

Fig. 10—Response of surface temperatures to casting speed change at 80 s into simulation: speed change 1.0 to 0.8 m/min, 152-mm-thick slab. Flow rates adjusted according to a prescribed spray table and by the control module.

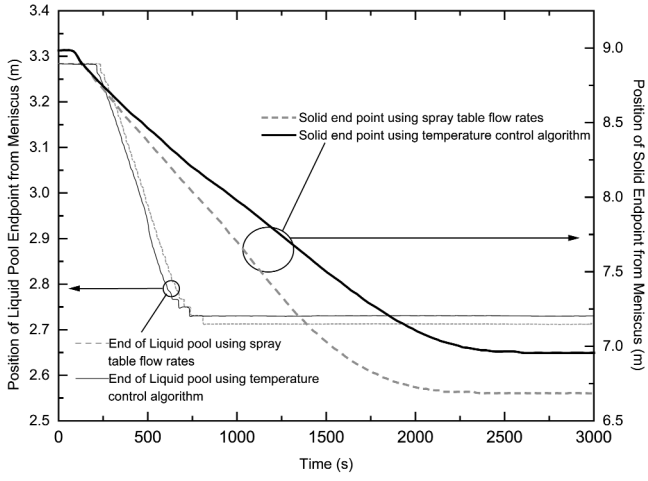

Fig. 11—Response of liquid pool depth and solidification end point to casting speed change at 80 s into simulation: speed change 1.0 to 0.8 m/min, 152-mm-thick slab. Flow rates are adjusted according to the prescribed spray table and by the control module.

table is used to set the flow rates, as shown in Figure 10. In the figure, legends for set-point positions are placed above steady-state results where the flow rates are adjusted according to casting speed table. When the spray table is used, the temperature initially increases as the surface responds quickly to the reduced water flow prescribed at the lower speed. As time proceeds and the internal slab temperatures adjust to the new casting conditions, the slab surface cools to below its initial temperatures. Also given in Figure 10 are temperatures at the set points for the same casting speed change with the control system used to maintain the temperatures at their starting values. The control system works well and keeps the temperatures at their initial values.

The changes in liquid pool depth and solidification end point for the two cases discussed previously are given in Figure 11, where casting speed is changed from 1.0 to 0.8 m/min, using temperature control and the spray tables. Note that with both surface temperature control and the spray tables, there will be changes in these parameters because they are largely dependent on casting speed. When the casting

speed spray table is used, the final surface temperature is cooler than when temperature control is used and the changes in these parameters are larger. Unlike the case of casting speed increase, the response times for liquid pool depth and solidification end point to reach their final conditions are substantially longer than the time required for propagation from the meniscus at the new casting speed. The response times of the liquid pool depth and the solidification end point to reach steady state are about 800 and 2500 seconds after the speed reduction, respectively. The times required for the first steel entering the mold at the new, reduced speed (0.8 m/min) to propagate from the meniscus to the new liquid pool depth (about 2.73 m) and to the new solid end point (about 6.9 m) are about 205 and 517 seconds, respectively. When the casting speed is slowed, the new thermal conditions take considerably longer to arrive at their new state than if the machine were sped up. The new liquid pool and solid end point move up the caster, opposed by the casting speed. By contrast, when the machine is sped up, the new liquid pool and solid end point positions propagate with the casting speed to their new positions. Other computational studies have shown that, for the same absolute casting speed change, the solidification conditions require a factor of 4 or 5 times longer to come to equilibrium when the speed is decreased *vs* a casting speed increase.

D. *Results of Preliminary Real-Time Version of DYSCOS Model*

Execution time depends on the grid used, the rate at which casting conditions are changing, and other computational factors, such as steel composition if the microsegregation solidification model is used (number of elements and their concentrations). To achieve real-time or faster execution speeds, the grid is made coarser and less detail is used in describing the boundary conditions (*i.e.,* no individual roll contacts). To speed execution, half the slab thickness can be modeled, symmetry about the slab thickness can be assumed, and the prescribed temperature-solid fraction relations may be used. When this latter option is used, execution speed is around 20 to 25 pct faster than using the microsegregation solidification model, depending on the alloy composition. Nevertheless, the model is capable of running in real time without using prescribed temperature-solid fraction relations.

In Figure 12(a), solid fraction contours are presented for the offline detailed DYSCOS model, and in Figure 12(b), the result for a real-time run of the model is presented, where real-time (and faster) execution speed was achieved using the DYSCOS solidification model. Casting conditions are the same, but the detailed model in Figure 12(a) uses a 3000 by 90 grid, and the real-time model in Figure 12(b) uses a 200 by 18 grid. The model in Figure 12(a) requires 4 to 20 times real time to run depending on the casting conditions, and the detailed model in Figure 12(b) required 0.25 to 1 times real time to execute using the same casting speed changes and other conditions. Reported execution time here is for a 500 MHz Alpha 21264 CPU workstation with 1 GB RAM.

The solidification profiles shown in Figure 12 were different between the two models. The effect of the grid is apparent in the results shown in Figure 12(b). The end of liquid core occurs at 4.67 and 3.94 m from meniscus for the higher detail and real-time DYSCOS models, respectively. The end of

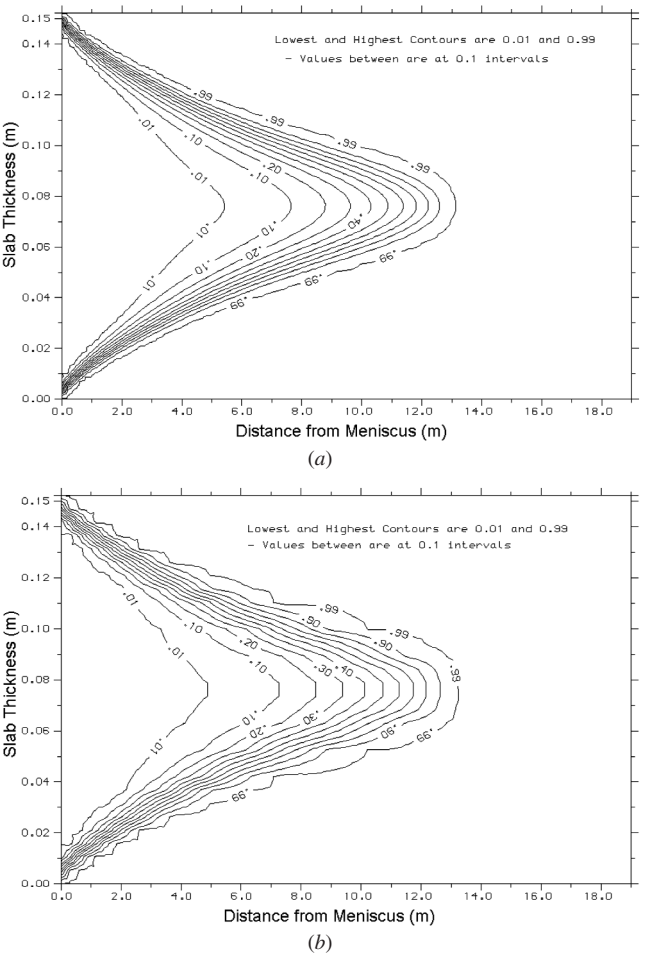

Fig. 12—(*a*) Solid fraction contours for the DYSCOS model using a grid of 3000 axial cells by 90 thickness cells. (*b*) Solid fraction contours for the real-time version of the DYSCOS model using a grid of 200 axial cells by 18 thickness cells.

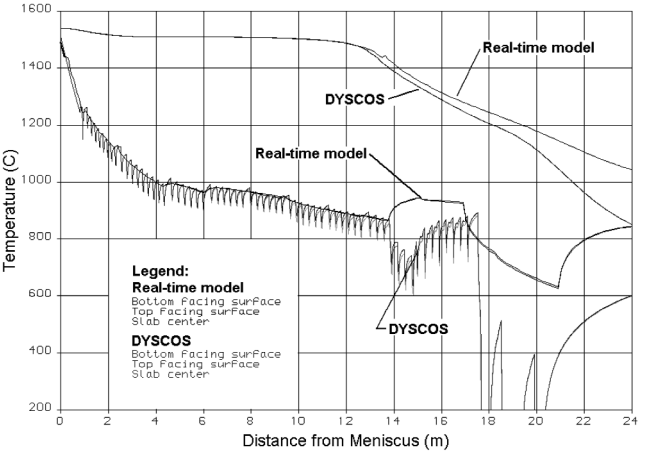

Fig. 13—Comparison between slab centerline and surface temperature profiles for the model using a real-time (200 × 18) grid and using the DYSCOS high detail grid (3000 × 90) running slower than real time.

solidification occurs at 13.31 m from meniscus for the higher detail model and at 13.64 m from meniscus for the real-time DYSCOS model. A comparison of temperature profiles for the higher detail and real-time DYSCOS models is shown in Figure 13. A comparison of temperature at the unbending

point of the machine (14.25 m from meniscus) gives about 740 °C for the high detail DYSCOS model and 928 °C for the real-time model. Up to about 14 m, the model temperatures agree. At positions after that, the effect of taking area averaged boundary conditions for the lower machine segments results in large disparities. When quenching is used, starting at around 17.5 m, the quench-region temperatures show large disagreement. This indicates the kind of realism that is lost by taking "averaged" boundary conditions in the segments and neglecting the banks of spray nozzles and contacting rolls. Another method of computing the boundary conditions is required for better agreement when using the real-time model after the unbending region, and in regions with higher flow rates. Handling localized effects such as the Leidenfrost transition temperature should be taken into account in the coarse real-time model. These issues and further development of the real-time model are topics for future investigations.

IV. CONCLUSIONS

Using steady-state calibration factors, comparisons between measured and predicted surface temperatures show that the predictions are, on average, within ±30 °C of the measurements for the transient model presented here. Parametric studies demonstrate the differences in the thermal and solidification responses of the slab for casting speed increases and decreases. Temperature variations that occur when a spray cooling table is used to prescribe the flow rates as a function of casting speed have been presented. A control method that maintains slab surface temperatures within desired ranges was developed and simulated. The DYSCOS model is a valuable computational tool and accurate simulator for investigating transient phenomena in slab caster operations, and for developing control methods. As part of future work, a real-time control module should be completed and tested using numerical experiments performed using the high detail DYSCOS model. Using the high detail DYSCOS model as a realistic predictor, this work could proceed with limited machine trials. A real-time control version of the model would also require periodic online calibration, and it is planned that such a dynamic calibration capability will be implemented in the high-detail and real-time DYSCOS models as part of future work.

ACKNOWLEDGMENTS

The authors gratefully acknowledge their sponsors, IPSCO Inc., for their support of this research program. In particular, the efforts of Dr. Laurie Collins and Mr. Jonathan Dorricott in promoting this collaboration are greatly appreciated. Also, the assistance provided by Mr. Brian Wales in supplying additional caster operating and temperature data is greatly appreciated.

REFERENCES

1. W.R. Irving: *Continuous Casting of Steel,* Institute of Metals, London, 1993, pp. 182–85.
2. K. Okuno, H. Naruwa, T. Kuribayashi, and T. Takamoto: *Iron Steel Eng,* 1987, vol. 12 (4), pp. 34–38.
3. K.-H. Spitzer, K. Harste, B. Weber, P. Monheim, and K. Schwerdtfeger: *Iron Steel Inst. Jpn.* 1992, vol. 32 (7), pp. 848–56.
4. S. Barozzi, P. Fontana, and P. Pragliola: *Iron Steel Eng.,* 1986, vol. 12, pp. 21–26.
5. S. Louhenkilpi, E. Laitinen, and R. Nienminen: *Metall. Trans. B,* 1993, vol. 24B, pp. 685–93.
6. J. Miettinen: *Metall. Trans. B,* 1997, vol. 28B, pp. 281–97.
7. J. Miettinen and S. Louhenkilpi: *Metall. Trans. B,* 1994, vol. 25B, pp. 909–16.
8. S. Louhenkilpi: *Acta Polytechnica Scandinavica,* Chemical Technical Series No. 230, The Finish Academy of Technology, Finland, 1995.
9. K. Mörwald, K. Dittenberger, and K.D. Ives: *Ironmaking Steelmaking,* 1998, vol. 25 (4), pp. 323–27.
10. T. Takawa, R. Takahashi, and M. Tatsuwaki: *Sumitomo Search,* 1987, vol. 34, pp. 79–87.
11. R.D. Pehlke, A. Jeyarajan, and H. Wada: "Summary of Properties for Casting Alloys and Mold Materials," Report NSF/MEA-82028, National Technical Information Service, Washington, DC, 1982.
12. R. Hardin and C. Beckermann: *ASME Nat. Heat Transfer Conf. Proc.,* 1997, HTD-vol. 347, pp. 9–20.
13. A.A. Howe: *Ironmaking and Steelmaking,* 1988, vol. 15 (3), pp. 134–42.
14. M.C. Schneider and C. Beckermann: *Metall. Mater. Trans. A,* 1995, vol. 26A, pp. 2373–88.
15. C.Y. Wang and C. Beckermann: *Metall. Trans. A,* 1993, vol. 24A, pp. 2787–802.
16. C.Y. Wang and C. Beckermann: *Mater. Sci. Eng.,* 1993, vol. A171, pp. 199–211.
17. *A Guide to the Solidification of Steels,* Jernkontoret, Stockholm, 1977.
18. Y.S. Touloulian, R.W. Powell, C.Y. Ho, and P.B. Klemens: *Thermophysical Properties of Matter,* IFI/Plenum, New York, NY, 1972, vol. 8.
19. T. Nozaki, J.I. Matsuno, K. Murata, H. Ooi, and M. Kodama: *Trans. Iron Steel Inst. Jpn.,* 1978, vol. 18 (6), pp. 330–38.
20. L. Bolle and J.C. Moureau: *Int. Conf. on Heat and Mass Transfer in Metallurgical Processes,* Dubrounik, Yugoslavia, 1979, pp. 527–34.
21. E. Laitinen and P. Neittaanmäki: *Control-Theory Adv. Technol.,* 1988, vol. 4 (3), pp. 285–305.
22. M. El-Bealy, N. Leskinen, and H. Fredriksson: *Ironmaking and Steelmaking,* 1995, vol. 22 (3), pp. 246–55.
23. R. York and H.K. Spitzer: *Solidification Processing 1997—Proc. 4th Decennial Int. Conf. on Solidification Processing,* Dept. of Engineering Materials, University of Sheffield, UK, 1997, pp. 163–65.
24. C.L. De Bellis and S.E. Le Beau: *1989 ASME Nat. Heat Transfer Conf. Proc.,* 1989, HTD-vol. 113, pp. 105–11.
25. F. Kreith and M. Bohn: *Principles of Heat Transfer,* 5th ed., West Publishing Co., St. Paul, MN, 1993, p. 329.